Hydraulically Drained Flows in Rotating Basins. Part II: Steady Flow

LAWRENCE J. PRATT

Woods Hole Oceanographic Institution, Woods Hole, Massachusetts

(Manuscript received 31 December 1995, in final form 23 July 1996)

ABSTRACT

The slow, horizontal circulation in a deep, hydraulically drained basin is discussed within the context of reduced-gravity dynamics. The basin may have large topographic variations and is fed from above or from the sides by mass sources. Dissipation is provided by bottom friction. To the order of the appromixations made (weak forcing and dissipation), the nonlinear hydraulic control is found to influence only the mean level of the interface separating upper and lower layers, and not the horizontal circulation. For the case of forcing from above the interior basin flow is anticyclonic about closed geostrophic contours and feeds into diffusive boundary layers leading to the draining strait and sill. With sidewall forcing, the interior is motionless and flow is channeled directly to the strait in boundary layers. The latter may circle the basin cyclonically or anticyclonically depending on the source distribution, and a circulation integral is shown to predict the sense of the overall swirl velocity and the presence of eastern and western boundary currents. Modifications caused by the presence of open geostrophic contours or horizontal friction are commented upon. The model is used to predict pathways for deep flow entering the Norwegian Sea from the Greenland Sea and escaping through the Faroe–Shetland Channel. Comparison with the few existing observations are made.

1. Introduction

Part I of this work (Pratt and Llewellyan Smith 1997) establishes an analytical method for computing deep, reduced-gravity circulations contained in deep basins and drained through a strait acting as a hydraulic control. The main approximations allowing analytical tractability are 1) the strait and sill system allows only a weak outflow compared to the recirculating mass in the interior of the basin and 2) that forcing and dissipation are equally weak. Although the outflow is weak, the strait and sill potentially have a zero-order influence on the basin circulation. This influence is exercised through slow time dependence in the amplitudes of the oscillating and steady (geostrophic) modes that make up the circulation. The purpose of this article is to explore the simplest case of hydraulically drained flow, namely, that of steady flow in the upstream basin. Specifically, the interior circulations, interface configurations, and boundary currents that arise when the deep fluid is fed from above or from the side by a mass source that crudely approximates deep convection in the overlying fluid, sinking of fluid on the surrounding shelf, or inflows from neighboring basins will be illustrated. To the extent permitted by existing observations, comparisons are made with the circulation of deep and intermediate waters in the Nordic seas.

Of particular interest are the features of the interior circulation influenced by the hydraulic control. It will be shown that the only significant interior feature subject to regulation by the control is the mean stratification, that is, the mean elevation of the interface separating upper and lower fluids. The interior horizontal circulation can be specified independently of the boundary conditions around the edge of the basin, which takes the strait and sill out of play. For the case of an interior mass source, the horizontal circulation directs the added mass slowly into boundary currents, which carry it to the entrance of the strait. The general dynamics of the boundary currents are independent of the hydraulic control, although the detailed velocity structure may depend on the velocity distribution at the strait entrance, which in turn is influenced by the hydraulics.

Also of interest are the pathways of flow between the source and the sill. In general, the trajectories of fluid parcels introduced into the basin are sensitive to the type of source (interior or sidewall) and to the type of geostrophic contour (open or closed) on which the fluid is introduced. A circulation integral about the basin edge can be used to predict the overall sense (cyclonic or anticyclonic) of the boundary circulation.

A brief review of the governing equations and approximations is given in the next section. Included are the integral constraints that govern the interior circulation and interface elevation. Section 3 explores interior solutions for a circular basin with radially varying bot-

Corresponding author address: Dr. Lawrence J. Pratt, Woods Hole Oceanographic Institution, Woods Hole, MA 02543.
E-mail: lpratt@whoi.edu

tom topography, including cases of interior and of sidewall mass sources. It is here that the hydraulic control of the stratification is established. For an interior mass source the interior circulation is anticyclonic about geostrophic contours and the added fluid must be carried out of the interior by a weaker, ageostrophic circulation. Introducing a weak bottom drag gives rise to an $O(\varepsilon)$ radial velocity, which, depending on one's view of the drag law, may be thought of as an ageostrophic interior velocity or an Ekman flux. (The small parameter ε measures the strength of the outflow and is the same order as the Rossby number.)

The ageostrophic secondary circulation (discussed in section 4) carries fluid to the basin boundaries and from there it must be diverted to the entrance of the strait by a boundary layer. If the mass is introduced through the sidewalls, there is no interior circulation and the fluid is carried directly to the strait by the boundary layer. As shown in section 5, the boundary layer obeys the same diffusion equation that governs the northern or southern boundary layer in a Stommel model (Pedlosky 1968, 1974) or the ''arrested topographic wave'' of Csanady (1978). In order to calculate the detailed velocity structure in this layer, it is necessary to specify the velocity profile of fluid entering the strait, which in turn requires some analysis of the hydraulic model (section 6). The solution is then given (section 7) for the case of a sidewall mass source, which gives cyclonic flow around most of the basin edge with an overshoot at the entrance. An interior mass source also gives a cyclonic boundary layer circulation but this is overwhelmed by the anticyclonic interior velocity field.

Section 8 comments on the potential vorticity of the outflow, whose value is shown to be a decreasing function of transport. This feature is consistent with recent work (Killworth 1994) indicating zero potential vorticity as a condition for maximal transport. Section 9 explores modifications of the circulation that occur when open geostrophic contours are introduced into the interior. The resulting combination of Sverdrup and ''circumpolar'' interiors with associated diffusive and Stommel western boundary layers gives rise to interesting and rich path structures. A brief note on the structure of the interior flow and boundary layer under the presence of horizontal friction, rather than bottom friction, is presented in section 10. Section 11 discusses possible connections with the horizontal circulation of intermediate and upper deep water in the Greenland, Iceland, and Norwegian Seas. Finally, section 12 generalizes the discussion of circulation sense and, in particular, the presence of eastern versus western boundary currents, by making use of a circulation integral.

2. Review of governing equations

Consider a basin containing a deep, reduced-gravity layer that is fed either from the side (Fig. 1a) or from above (Fig. 1b) and drains through a strait. A quiescent

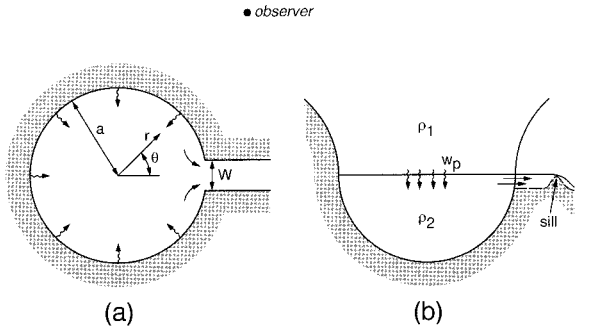

FIG. 1. Definition sketch with (a) showing a plan view with mass introduced from the sidewalls and (b) showing a vertical cross section with fluid fed from above.

state is possible when the interface lies at sill level, in which case the dimensional lower layer thickness is denoted $H(x, y)$. Nondimensional quantities are obtained using the scale depth H_o, the (constant) Coriolis parameter f_o, and the interface displacement scale N to form the length scale $L_d = (gH_o)^{1/2}/f_o$ and the velocity scale $(gH_o)^{1/2}N/H_o$. The resulting dimensionless equations for momentum and mass conservation are

$$\mathrm{Ro}(\mathbf{U}\cdot\boldsymbol{\nabla})(\mathrm{U}H_o/H) + \mathbf{k}\times\mathbf{U} = -(H_o/H)\boldsymbol{\nabla}\eta + \varepsilon\mathbf{F} \tag{2.1}$$

$$\boldsymbol{\nabla}\cdot\mathbf{U} + \mathrm{Ro}\boldsymbol{\nabla}\cdot(\eta\mathbf{U}H_o/H) = \varepsilon w_p, \tag{2.2}$$

where $\mathbf{U}$ is the vector transport (depth-integrated horizontal velocity) and η is the displacement of the interface above sill level. Also, Ro is the Rossby number ($=N/H_o$ under the above scaling), ε is a small nondimensional parameter measuring the degree of constriction of the sill or width contraction, $\mathbf{F}$ represents friction, and w_p represents a positive downward, interfacial entrainment velocity acting in the basin interior. The presence of the coefficient ε in the friction and entrainment terms reflects the basic assumption of weak forcing and dissipation.

For Ro and $\varepsilon \ll 1$ the interior circulation is geostrophic and follows H/H_o contours (f/H contours dimensionally). After expansion in powers of ε (i.e., $\eta = \eta_g + \varepsilon\eta^{(1)} + \ldots$) the lowest order velocity and thickness fields are calculated using compatibility conditions, here obtained by setting the right-hand sides of Eqs. (4.10) and (4.13) in Part I equal to zero:

$$\iint_{A_C} \mathbf{k}\cdot\boldsymbol{\nabla}\times(\mathbf{F}H_o/H)\,d\sigma = (H_o/H)\iint_{A_C} w_p\,d\sigma \tag{2.3}$$

and

$$\int_0^W \mathbf{U}^{(1)}\cdot\mathbf{n}\,ds = \iint_A w_p\,d\sigma = T, \tag{2.4}$$

where A_C is the area enclosed by any H/H_o contour C,

all of which are assumed closed, and A is the basin area. [Note that the f-plane assumption is enforced by setting $f = 1$ in (4.1) of Part I and that the nonlinear terms are zero as explained in the remarks following that equation.] Equation (2.3) is the circulation integral equating the squashing of fluid columns by positive w_p within A_C by frictional torque acting around the edge of A_C. Equation (2.4) is simply the mass balance for the basin for the case of an interior mass source, with the middle term representing the integral over the strait entrance width W of the outflow transport velocity $\mathbf{U}^{(1)}\cdot\mathbf{n}$.

In a hydraulically controlled flow, the outflow transport, T, is nonlinearly linked to the geometry of the sill or width contraction and to other independent flow variables. The formulation used in Part I is due to Whitehead et al. (1974, hereafter referred to as WLK) and requires the constriction parameter ε to be O(Ro). The WLK model gives the following outflow transport, T, relationship:

$$T = \left(\frac{2}{3}\right)^{3/2} w_s \left[\eta_r - \frac{w_s^2}{8}\right]^{3/2}, \tag{2.5}$$

where η_r is the value of η_g measured at the right-hand corner of the entrance (facing into the strait) and $w_s = \mathrm{Ro}^{-1/2} W_s$ [$= O(1)$] with W_s representing the dimensionless channel width at the sill, the cross section being rectangular. Equation (2.5) follows directly from (5.2a) of Part I [also see (5.3a)] and involves a number of assumptions. For present purposes it is sufficient to repeat that the formula is valid as long as the lower layer thickness remains finite across the entire channel width at the sill. In principle, the sill flow may separate from the left-hand side of the channel, in which case (2.5) is replaced by another formula [see (5.3b) of Part I]. However, the possibility of separated sill flow in a hydraulically controlled environment with smoothly varying, rectangular geometry has been questioned by Pratt (1987) [also implicit in Shen (1981)] and will not be considered here. For further details regarding the underlying assumptions, the reader should consult Part I.

3. The interior circulation

Suppose now that friction takes the form of bottom drag, so that $\mathbf{F} = -R_f \mathbf{u}_g$ in (2.3), where $\mathbf{u}_g$ is the vector geostrophic velocity. This frictional law may be interpreted as originating from a linear drag law with dimensional drag coefficient D_f, leading to $R_f = D_f/\mathrm{Ro} f_o H_o$, or from an Ekman model with $D_f = f_o(A_v/2f_o)^{1/2}$, A_v being the vertical eddy viscosity. In general, $\mathbf{F}$ will also include a term accounting for momentum transfer from upper to lower layer due to w_p. Under present scaling assumptions, that term is $O(\varepsilon\mathrm{Ro})$ and is therefore negligible.

Applying these definitions to (2.3) and using Stokes's theorem to simplify the right-hand side leads to

$$\oint_C \mathbf{u}_g\cdot\mathbf{l}\, ds = -\frac{1}{R_f}\iint_{A_C} w_p\, d\sigma \le 0, \tag{3.1}$$

showing that the circulation averaged about geostrophic contours is anticyclonic, a result independent of the basin shape. Anticyclonic circulation is also a feature of the lower layer flow of a two-layer system driven by a mass transfer from the upper to the lower layer (Gill et al. 1979). [In contrast, Kawase and Straub (1995, manuscript submitted to *J. Phys. Oceanogr.*) argue that abyssal circulation about closed geostrophic contours is generally cyclonic if the flow is driven by a lateral influx of mass.]

For the case of a circular basin of radius a [and using cylindrical coordinates (r, θ) and radial and azimuthal velocities (u, v), as shown in Fig. 1a] suppose that w_p has a finite, uniform value for $r < r_o$ and is zero for $r > r_o$. Thus,

$$w_p = \begin{cases} T/\pi r_o^2, & r \le r_o \\ 0, & r > r_o, \end{cases} \tag{3.2}$$

and the corresponding azimuthal velocity is given by (3.1) as

$$v_g = \frac{-1}{2\pi r R_f}\begin{cases} r^2 T/r_o^2, & r \le r_o \\ T, & r > r_o. \end{cases} \tag{3.3}$$

From the geostrophic relation $v_g = \partial\eta_g/\partial r$ and the corresponding interface elevation is therefore

$$\eta_g(r) = \eta_g(a) - \frac{T}{2\pi R_f}\begin{cases} \ln(r_o/a) + (r^2 - r_o^2)/2r_o^2, \\ \qquad r \le r_o \\ \ln(r/a), \\ \qquad r > r_o. \end{cases} \tag{3.4}$$

To find $\eta_g(a)$ the hydraulic law (2.5) is inverted, leading to

$$\eta_g(a) = \frac{3}{2}(T/w_s)^{2/3} + w_s^2/8. \tag{3.5}$$

Figure 2a shows $\eta_g(r)$ for the settings $T = 1$, $a = 1$, $r_o = \frac{1}{2}$, $R_f = 0.2$, and $w_s = 0.5$, over a diameter of the circular basin. From this figure, and (3.4) and (3.5), one can identify the following features: First, the horizontal circulation is anticyclonic about closed geostrophic contours with the interface forming a dome. The magnitude of the velocity is independent of the topography. In the source region, $r < r_o$, the interface has negative curvature ($\partial^2\eta_g/\partial r^2 = -w_p$), while outside the curvature is positive ($\partial^2\eta/\partial r^2 = T/2\pi r^2$). These features are also shown in Fig. 2b, where a has been increased to 4. Finally, only the ''base'' interface elevation $\eta_g(a)$ is determined by the hydraulic control. If the sill width w_s or elevation (from which η_g is measured) is varied, the interface will

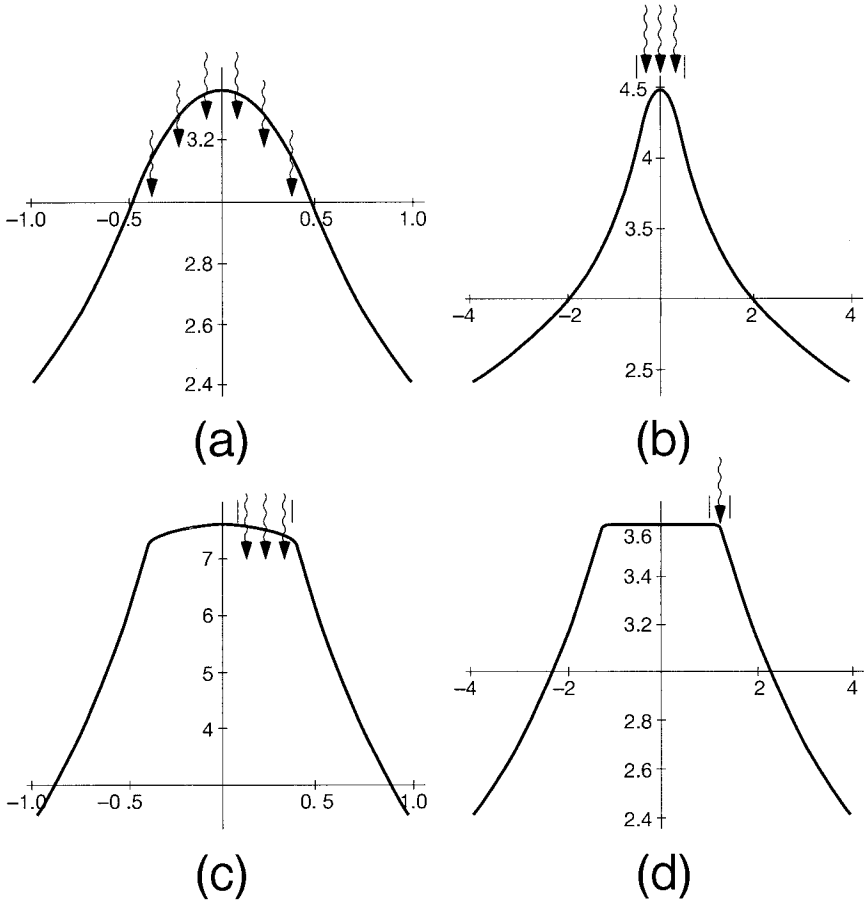

FIG. 2. Interface elevation above sill over diameter ($-a < r < a$) of circular basin for $T = 1$, $R_f = 0.2$, $a = 1$, and $W = W_s = 0.5$. For (a) the source region lies within $r < r_o = 0.5$ and $a = 1$. In (b) a has been increased to 4. For (c) $a = 1$ and the source lies within $0.1 = r_1 < r < r_2 = 0.4$. and $0 < \theta < \theta_o$, where θ_o is arbitrary. In (d) r has been increased to 4, $r_1 = 1.1$, and $r_2 = 1.4$,

move up or down as a whole, but spatial variations of the interface will remain fixed.

For nonaxisymmetrical forcing (but still circular geostrophic contours) v_g and η_g remain axisymmetrical with the former given by the $2\pi r$ times the right-hand side of (3.1) and the latter by the geostrophic relation. For example, an isolated patch of finite w_p occupying $r_1 < r < r_2$ and $0 < \theta < \theta_1$ leads to the interface displacement

$$\eta_g(r) = \eta_g(a) + \frac{T}{2\pi R_f D}\begin{cases}\frac{1}{2}(r_2^2 - r_1^2) + r_1^2(\ln(r_1) - \ln(r_2)) + \ln(a) - \ln(r_2), & r < r_1 \\ \frac{1}{2}(r_2^2 - r^2) + r_1^2(\ln(r) - \ln(r_2)) + \ln(a) - \ln(r_2), & r_1 < r < r_2 \\ \ln(a) - \ln(r), & r > r_2,\end{cases}$$

where $D = r_2^2 - r_1^2$. The displacement field is shown in Fig. 2c using the same parameters as in Fig. 2a and $r_1 = 0.1$ and $r_2 = 0.4$. Over the geostrophic contours crossing the source region (those occupying $r_1 < r < r_2$) the interface again has negative curvature ($\partial^2\eta/\partial r^2 = -T(r^2 + r_1^2)/2\pi r^2 D$) while outside the curvature is again positive ($\partial^2\eta/\partial r^2 = T/2\pi r^2$). The calculation is repeated with $a = 4$, $r_1 = 1.1$, and $r_2 = 1.4$ and the results shown in

Fig. 2d. The positive and negative curvature regions associated with nonsource and source regions might make it possible to distinguish such regions using hydrographic sections.

In some oceanographic applications, the overflowing layer overlies a deeper, stagnant layer and contact with the bottom is lost except at the basin edge. This situation apparently occurs in the Norwegian Sea where overflow water is thought to comprise primarily intermediate and upper deep water types (Hopkins 1991). The calculations presented above are still applicable with three modifications. First, the definition of the reduced gravity must be altered slightly. Second, friction must be interpreted as an interfacial drag. Finally, since the H/H_o is nearly constant, any closed contour qualifies as a geostrophic contour and (2.3) must replaced by the quasigeostrophic potential vorticity equation, as described in section 4c of Part I. However, solutions of this equation for the forcing functions given above are identical to those already presented, as suggested by the fact that H does not appear in the latter.

We conclude this section with the obvious remark that, if fluid is fed into the basin through the sidewalls, rather than across the interface, (3.1) requires the interior geostrophic velocity to be zero at all points.

4. The secondary circulation

How does the fluid make its way from the source to the strait? Since the radial geostrophic velocity is zero, the outward transport must be carried by the ageostrophic velocity component $u^{(1)}$. The latter may be found from the steady form of the $O(\varepsilon)$ momentum and continuity equations, (3.1) and (3.2) of Part I, which reduce to

$$\mathbf{k} \times \mathbf{U}^{(1)} + \frac{H}{H_o}\nabla\eta^{(1)} = \mathbf{F}$$

and

$$\nabla\cdot\mathbf{U}^{(1)} = w_p,$$

under current assumptions. Writing these in polar coordinates and eliminating $v^{(1)}$ and $\eta^{(1)}$ leads to

$$u^{(1)}\frac{\partial}{\partial r}\frac{H}{H_o} = w_p + \frac{HR_f}{rH_o}\frac{\partial}{\partial r}\left(rv_g\frac{H_o}{H}\right), \qquad (4.1a)$$

which is valid for axisymmetric topography. A useful alternative form can be obtained by expanding the derivative in the final term and making use of (3.1), leading to

$$u^{(1)} = \left[w_p - (2\pi r)^{-1}\oint_C rw_p\, d\theta\right]\left(\frac{\partial}{\partial r}\frac{H}{H_o}\right)^{-1} - v_gR_f\frac{H_o}{H}. \qquad (4.1b)$$

If w_p is independent of θ, the first term on the right-hand side of (4.1b) vanishes and the radial velocity reduces to $-v_gR_fH_o/H$. If the linear drag is felt uniformly throughout the water column, this last expression represents an ageostrophic velocity distributed uniformly over depth. With the Ekman model interpretation $-v_gR_fH_o$ represents the volume flux in the bottom boundary layer. In either case the radial velocity may be calculated independently of the boundary conditions, and there is no guarantee that the condition of zero normal transport at the basin edge will be satisfied. For example, the forcing (3.2) leads to

$$u^{(1)}(a,\,\theta) = T/(2\pi aH(a)/H_o), \qquad (4.2)$$

if (4.1b) is used with (3.1). (This result could also have been derived using mass conservation alone.) A boundary layer is clearly needed to divert this flow into the strait, a subject taken up next.

5. The boundary layer

Denoting the thickness of the hypothetical boundary layer by δ and recognizing that the layer must bring the $O(\varepsilon)$ radial transport to zero at $r = a$ and divert this flow along the boundary into the strait, it is anticipated that the radial boundary-layer velocity u_B must be $O(\varepsilon)$, while the azimuthal velocity v_B must be $O(\varepsilon/\delta)$. Since the WLK model requires $\varepsilon = O(\mathrm{Ro})$, we henceforth replace ε by Ro. The full velocity and displacement fields for the circular basin may therefore be written as

$$\begin{aligned} u &= \mathrm{Ro}u_B(\xi,\,\theta) + \mathrm{Ro}u^{(1)}(r,\,\theta) + \cdots \\ v &= v_g(r) + (\mathrm{Ro}/\delta)v_B(\xi,\,\theta) + \mathrm{Ro}v^{(1)}(r,\,\theta) + \cdots \\ \eta &= \eta_g(r) + \mathrm{Ro}\eta_B(\xi,\,\theta) + \mathrm{Ro}\eta^{(1)}(r,\,\theta) + \cdots, \end{aligned} \qquad (5.1)$$

where $\xi = (a - r)/\delta$.

The rapidly varying boundary-layer fields lie outside the classes of flows considered in Part I and the governing equations must be derived from basics. Forming a potential vorticity equation from (2.1) and (2.2) in the usual manner leads to

$$\frac{d}{dt}\left(\frac{1 + \mathrm{Ro}\zeta}{(H/H_o) + \mathrm{Ro}\eta}\right) = \frac{\mathrm{Ro}}{(H/H_o + \mathrm{Ro}\eta)}\left[\mathbf{k}\cdot\nabla\times(\mathbf{F}H_o/H) - w_p\frac{(1 + \mathrm{Ro}\zeta)}{(H/H_o + \mathrm{Ro}\eta)}\right], \qquad (5.2)$$

where ζ represents relative vorticity and ε has been replaced by Ro as explained earlier. After substitution of (5.1), careful expansion of the result, and subtraction of the vorticity balances for the interior geostrophic and ageostrophic fields, one obtains

$$u_B\frac{\partial}{\partial r}\left(\frac{H_o}{H}\right) + \frac{\mathrm{Ro}^2}{\delta^3}\left(\frac{H_o}{H}\right)(u_B + u^{(1)})\frac{\partial^2 v_B}{\partial \xi^2} - \frac{\mathrm{Ro}}{\delta^2 r}\left(\frac{H_o}{H}\right)\left(v_g - \left(\frac{\mathrm{Ro}}{\delta}\right)v_B\right)\frac{\partial^2 v_B}{\partial \xi \partial \theta} - \frac{\mathrm{Ro}R_f}{\delta^2}\left(\frac{H_o}{H}\right)^2\frac{\partial v_B}{\partial \xi} = 0.$$

Balancing the first term with the $O(\mathrm{Ro}/\delta^2)$ terms gives $\delta = \mathrm{Ro}^{1/2}$, rendering the remaining terms small. Dropping the latter and using

$$\frac{\partial}{\partial r}\left(\frac{H_o}{H}\right) = -\left(\frac{H_o}{H}\right)^2\frac{\partial}{\partial r}\left(\frac{H}{H_o}\right)$$

gives

$$u_B\frac{\partial}{\partial r}\left(\frac{H}{H_o}\right) + \frac{v_g}{r}\left(\frac{H}{H_o}\right)\frac{\partial^2 v_B}{\partial \xi \partial \theta} + R_f\frac{\partial v_B}{\partial \xi} = 0. \quad (5.3)$$

Unless $H(r)$ varies rapidly over the boundary layer, one may approximate $H(r)$ and its derivative by their values at $r = a$. Then, if $H(a)$ is zero, as is normally the case, (5.3) reduces to

$$u_B\left[\frac{\partial}{\partial r}\frac{H}{H_o}\right]_{r=a} + R_f\frac{\partial v_B}{\partial \xi} = 0. \quad (5.4)$$

Direct expansion of the momentum equation and subtraction of the $O(0)$ and $O(\mathrm{Ro})$ balances shows both boundary layer velocity components are geostrophic,

$$v_B = -\frac{\partial \eta_B}{\partial \xi} \quad (5.5)$$

and

$$u_B = -\frac{1}{a}\frac{\partial \eta_B}{\partial \theta}, \quad (5.6)$$

from which follows the condition of nondivergence:

$$\frac{\partial u_B}{\partial \xi} = \frac{1}{r}\frac{\partial v_B}{\partial \theta}. \quad (5.7)$$

Eliminating v_B between (5.3) and (5.5) leads to

$$\alpha^2\frac{\partial u_B}{\partial \theta} + \left(\gamma\frac{\partial}{\partial \theta} - 1\right)\frac{\partial^2 u_B}{\partial \xi^2} = 0, \quad (5.8)$$

where

$$\alpha^2 = \frac{-1}{aR_f}\left[\frac{\partial}{\partial r}\frac{H}{H_o}\right]_{r=a} \quad (> 0) \quad (5.9)$$

and

$$\gamma = \frac{-1}{aR_f}\left[\frac{v_g H}{H_o}\right]_{r=a} \quad (> 0). \quad (5.10)$$

When $\gamma = 0$, as occurs whenever v_g or H vanishes at the basin edge, (5.8) reduces to a diffusion equation with θ playing the role of time. The corresponding boundary layer on a straight coast is sometimes referred to as the ''arrested topographic wave'' (Csanady 1978). It is also equivalent to the northern or southern boundary layer arising in a homogeneous Stommel circulation in a rectangular basin (with the beta effect replacing the topographic effect). As such it can be traced back to the work of Pedlosky [1974, his Eq. (8.1)] and Pedlosky [1968, his Eq. (6.3)].

The estimate of the thickness of the diffusive ($\gamma = 0$) boundary layer can be refined somewhat by replacing the original estimate $\delta = \mathrm{Ro}^{1/2}$ by $\delta = \mathrm{Ro}^{1/2}/\alpha$, which is equivalent to replacing α^2 by unity in the $\gamma = 0$ version of (5.8). Dimensionalizing this estimate results in the dimensional boundary-layer thickness

$$\tilde{\delta} = \tilde{a}^{1/2}\left[\frac{D_f}{H_o\beta_T}\right]^{1/2} = \tilde{a}^{1/2}\delta_S^{1/2}, \quad (5.11)$$

where

$$\beta_T = -f_o\frac{\partial}{\partial r}\frac{H}{H_o}$$

is the topographic version of β, $\tilde{a}$ is the dimensional basin radius, and δ_s is the Stommel western boundary layer thickness based on topographic beta. The presence of the basin radius in the definition has the following meaning. It is well known that a diffusive process causes spreading in proportion to the square root of the distance from a point source. In the present problem the point ''source'' could correspond to the strait entrance or to an isolated source on the side wall. In any case, the boundary layer should thicken in proportion to the square root of distance around the basin edge from the isolated source. Since this distance is at most $2\pi\tilde{a}$, the average thickness should be proportional to $\tilde{a}^{1/2}$. Finally, note that increasing θ is equivalent to increasing time in a standard heat equation; therefore, we expect the boundary layer to spread as one moves counterclockwise around the basin edge.

If H is nonzero at the boundary or the variation of $H(r)$ across the boundary layer is sufficiently rapid that $H(r)$ cannot be replaced by $H(a)$, the term multiplied by γ in (5.8) must be taken into consideration. This term introduces waves into the otherwise diffusive boundary layer. Specifically, a Fourier representation of the solution with sums of terms proportional to $\sin(n\theta)$ or $\cos(n\theta)$ will be controlled at large n by a balance between the two terms involving θ derivatives. Keeping only these terms and integrating with respect to θ yields

$$\frac{\partial^2 u_B}{\partial \xi^2} + \frac{\alpha^2}{\gamma}u_B = \kappa/\gamma,$$

where κ is a constant. Since α^2/γ is positive, the so-

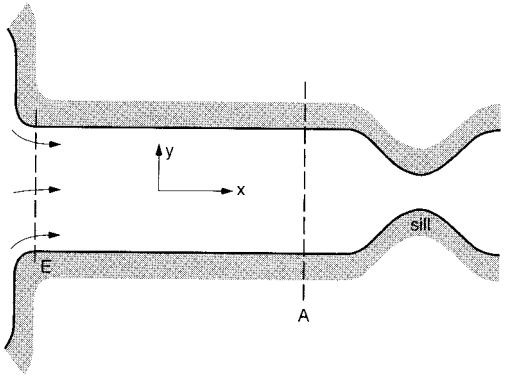

FIG. 3. Definition sketch showing entrance to strait (section E) leading into approach section (A), finally leading to sill section.

lutions oscillate, indicating the presence of topographic Rossby waves held stationary by the interior azimuthal velocity field. For the remainder of our discussion, attention will be focused on the purely diffusive ($\gamma = 0$) version of the boundary layer, which is the normal situation.

Solving (5.8) requires that u_B be specified all around the basin edge, including the strait entrance. WLK theory gives only the total transport and not the detailed velocity distribution at the strait entrance, and some further development is necessary to obtain the latter, a subject taken up next.

6. The boundary condition at the strait entrance

Figure 3 contains a diagram of the strait showing the entrance (section E) and an approach section (A) lying immediately upstream of the sill and width contraction. The cross section of the strait is assumed rectangular, as required by WLK, and the bottom elevation between sections A and E is assumed constant. Section E is positioned far enough downstream of the entrance that the flow entering the strait from the basin has become approximately parallel there. Furthermore, the same equations and scaling used in the basin are assumed to remain valid between sections E and A; the rapid, hydraulically driven flow occurring only downstream of A.

In dimensionless terms the potential vorticity of the fluid at section A is given by

$$q_A = \left[1 + \mathrm{Ro}(\zeta_g + \mathrm{Ro}\zeta^{(1)} + \cdots\right] \times \left[1 - \mathrm{Ro}\frac{H_o}{H_E}\left(\eta_g + \mathrm{Ro}\eta^{(1)} + \cdots\right)\right]\frac{H_o}{H_E}. \quad (6.1)$$

Now the volume transport into the strait is constrained by the hydraulic control to be $O(\mathrm{Ro})$, and therefore the lowest order normal velocity u_g at the entrance must either be zero, or net zero when integrated across the strait entrance. The second possibility is ruled out if the entrance coincides with a geostrophic contour, as is the case in the circular basin with finite topographic slope at $r = a$. It is therefore assumed that $u_g = 0$ across the entire entrance and that the same condition holds from the entrance to section A. Under these conditions ζ_g is zero in (6.1); therefore,

$$q_A \approx \left(1 - \mathrm{Ro}\eta_g\frac{H_o}{H_E}\right)\frac{H_o}{H_e}. \quad (6.2)$$

Since $u_g = 0$, η_g must be y independent and therefore q_A must be constant. Also, since η_g is constant along the side wall, it is equal to η_r [cf. Eq. (2.5)].

The flow from sections E to A is subject to bottom friction and therefore the entrance potential vorticity q_E may not equal q_A. A possible flow at E is one with uniform normal velocity and uniform relative vorticity. Since the potential vorticity of a fluid column flowing from E to A is altered in proportion to the relative vorticity, the potential vorticity of the flow would remain uniform across each cross section and would therefore reach a uniform state at A as required. Of course it must be verified that a flow with uniform normal velocity and uniform vorticity at E is dynamically consistent; this is done in connection with (6.3) below. Furthermore, such a flow is, at best, only a consistent entrance condition and may not hold up to a detailed analysis of the strait and corner regions. However, since the boundary layer is diffusive, its structure should not be too sensitive to the velocity profile imposed at the entrance provided that the entrance width is small, and that it is assessed more than a few widths away.

Since the basin boundary layer overlaps section E, the boundary layer fields must be taken into account in the computation of q_E. Using the boundary-layer scaling the result to $O(\mathrm{Ro})$ is

$$q_E = \left[1 + \mathrm{Ro}\left(\frac{\partial v_g}{\partial r} - \frac{\partial v_B}{\partial \xi} - \frac{H_o}{H_E}\eta_g\right)_{r=a} + O(\mathrm{Ro}^2)\right]\frac{H_o}{H_E}. \quad (6.3)$$

Since neither $\partial v_g/\partial r$ nor η_g vary across the strait entrance, uniform potential vorticity implies uniform $\partial v_B/\partial \xi$. By (5.4) the latter is proportional to the normal boundary-layer velocity u_B which, therefore, must also be uniform across the strait entrance. By mass conservation, u_B at the strait entrance takes on the following values depending on the mass source:

$$u_B(0, \theta) = \frac{TH_o}{WH_E}\left(1 - \frac{W}{2\pi a}\right) \quad \text{(interior forcing)} \quad (6.4)$$

or

$$u_B(0, \theta) = \frac{TH_o}{WH_E} \quad \text{(sidewall forcing)}. \quad (6.5)$$

Equations (6.4) or (6.5) give the normal boundary-layer velocity at the entrance.

In formulating the boundary condition around the remaining periphery of the basin further consideration of the geometry is required. Whether interior or sidewall sources of mass exist, a normal transport $u_B H/H_o$ must be specified at $r = a$, and the vanishing of $H(a)$ at the basin edge implies that $u_B \to \infty$ there. The vanishing of $H(a)$ also leads to some geometrical complexity near the corners of the strait entrance, where H takes the finite value H_e. Both problems can be avoided by simply assuming that the basin edge consists of a vertical wall such that $H(a) = H_e$. The diffusive limit ($\gamma \ll 1$) of the boundary layer balance then requires $H_e \ll H_o$.

7. Boundary layer solutions for interior and side wall sources

Using the entrance condition derived in the previous section, the solution can now be calculated for the diffusive ($\gamma = 0$) version of the boundary layer. The calculation is first performed for sidewall forcing with no interior mass source. A slight redefinition of coefficients then leads to the solution for the case of interior forcing. In the first case, the boundary condition at the entrance is given by (6.5). Around the remainder of the basin, the normal velocity is inward and is equal to the total transport T divided by the sidewall area $(2\pi a - W)H_E/H_o$. Thus,

$$u_B(0, \theta) = \frac{TH_o}{WH_e}\begin{cases} -W/(2\pi a - W), & |\theta| > W/a \\ 1, & |\theta| \le W/a, \end{cases} \tag{7.1}$$

assuming uniform inflow around the basin edge and using (6.5).

The general solution to (5.8) with $\gamma = 0$ may be written as

$$u_B(\xi, \theta) = \sum_{n=0}^{\infty} \left[A_n \cos\left(\alpha n^{1/2}\frac{\sqrt{2}}{2}\xi - n\theta\right) - B_n \times \sin\left(\alpha n^{1/2}\frac{\sqrt{2}}{2}\xi - n\theta\right)\right] e^{-\alpha n^{1/2}(\sqrt{2}/2)\xi}, \tag{7.2}$$

and the distribution (7.1) leads to $B_n = A_o = 0$ and

$$A_n = \frac{4TH_o a}{nH_e(2\pi a - W)W}\sin\left(\frac{nW}{\pi a}\right). \tag{7.3}$$

For the case interior forcing the boundary condition (7.1) is replaced by

$$u_B(0, \theta) = \frac{TH_o}{WH_e}\begin{cases} -W/2\pi a, & |\theta| > W/a \\ 1 - W/2\pi a, & |\theta| \le W/a \end{cases} \tag{7.4}$$

in view of (6.5). The solution (7.2) still holds but with

$$A_n = \frac{2TH_o}{WH_e\pi n}\sin\left(\frac{nW}{\pi\alpha}\right). \tag{7.5}$$

The zonal velocity and interface elevation for the boundary layer flow can be computed from (7.2) using (5.5)–(5.7), resulting in

$$v_B(\xi, \theta) = \frac{a\alpha}{\sqrt{2}}\sum_{n=1}^{\infty}\frac{A_n}{\sqrt{n}}\left[\sin\left(\alpha n^{1/2}\frac{\sqrt{2}}{2}\xi - n\theta\right) - \cos\left(\alpha n^{1/2}\frac{\sqrt{2}}{2}\xi - n\theta\right)\right] e^{-\alpha n^{1/2}(\sqrt{2}/2)\xi} \tag{7.6}$$

and

$$\eta_B(\xi, \theta) = a\sum_{n=1}^{\infty}\frac{A_n}{n}\sin\left(\alpha n^{1/2}\frac{\sqrt{2}}{2}\xi - n\theta\right)e^{-\alpha n^{1/2}(\sqrt{2}/2)\xi}. \tag{7.7}$$

Note that A_n, as defined by (7.3) and (7.5), are just multiples of each other, the multiplicative factor being independent of n, and the corresponding circulations therefore have identical streamline patterns but different flow speeds.

Figure 4a shows the streamlines ($\eta_B = \text{const}$) for the case of sidewall forcing using the same parameters as in Fig. 2a and with $\text{Ro}^{1/2} = 0.1$, $\alpha = 1$, $H_e/H_o = 0.2$, and $W = 0.5$. The basin is drained by a cyclonic boundary flow (lower part of figure) and, on the opposite wall, by an anticyclonic boundary flow. The cyclonic flow approaches the strait from the right (facing into the strait) and overshoots before entering. Some fluid penetrates into the interior.

In the above case, Fig. 4a, the basin radius is unity, which is convenient for displaying the solution but unrealistically small. Increasing the a to 4 leads to a solution with the same general path structure but more boundary layer character. A contour plot of this case is difficult to follow due to the dense packing of streamlines against the basin edge; instead, the azimuthal velocity profiles from the center to the edge are plotted for various values of θ in Fig. 4b. As before, the flow at the boundary is cyclonic for $\theta = \pi$ and $\theta = 3\pi/2$ and anticyclonic for $\theta = \pi/2$ ($\theta = 0$ marking the strait entrance). The boundary stagnation point separating cyclonic from anticyclonic flow is located at $(0.61 \pm 0.02)\pi$ for both $a = 1$ and $a = 4$.

The anticipated cyclonic spreading of the boundary current away from the strait can be detected in the streamline patterns Fig. 4. In Fig. 5 the same effect can be detected by following the outward migration of the zero crossings of the curves cyclonically from $\theta = \pi/2$ (top frame) to $\theta = 3\pi/2$ (bottom frame).

For the case of the interior mass source, the $O(\text{Ro}^{1/2})$

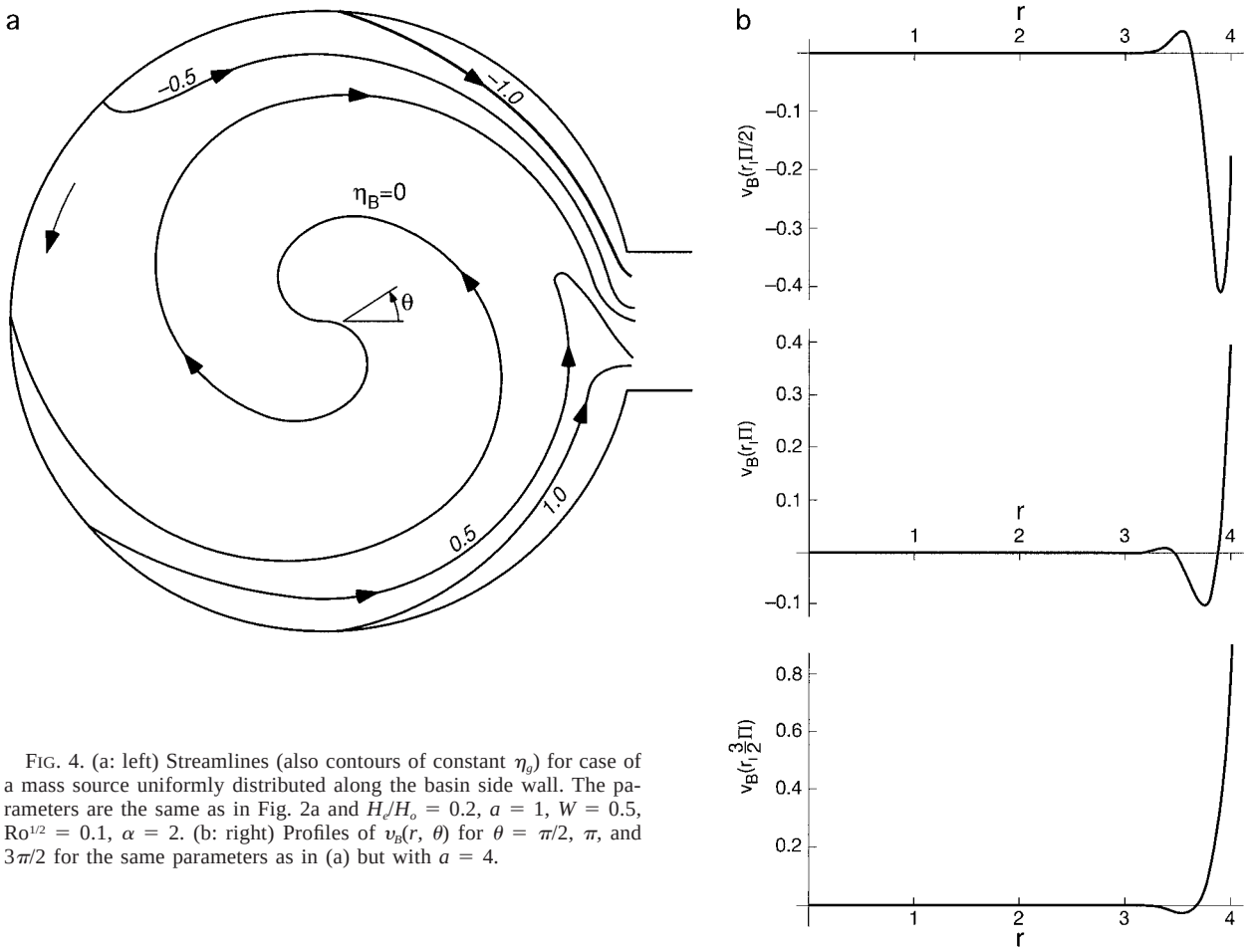

FIG. 4. (a: left) Streamlines (also contours of constant η_g) for case of a mass source uniformly distributed along the basin side wall. The parameters are the same as in Fig. 2a and $H_e/H_o = 0.2$, $a = 1$, $W = 0.5$, $\mathrm{Ro}^{1/2} = 0.1$, $\alpha = 2$. (b: right) Profiles of $v_B(r, \theta)$ for $\theta = \pi/2$, π, and $3\pi/2$ for the same parameters as in (a) but with $a = 4$.

azimuthal boundary layer velocity is dominated by the interior velocity, and the circulation patterns shown in Fig. 4 would be suppressed in a picture of the total circulation. The same remarks apply to the interface displacement, which is $O(\mathrm{Ro})$ in comparison. In Fig. 5 an exaggerated plot of the boundary layer interface displacement is shown above a plot of the interior displacement, below which is their sum. The parameters are the same as in Fig. 4 and the position of the observer relative to the strait entrance is indicated on Fig. 1. The upper plot was generated using (7.3) and (7.7) with $n = 15$. Since both solutions are geostrophically balanced, the velocity may be inferred from the surface slope. The boundary layer circulation is simply a scaled version of that shown in Fig. 4, while the interior circulation is anticyclonic. The strait entrance corresponds to the sharply sloping edge at the lower left-hand portion of the lower surface.

8. The relation between transport and potential vorticity

In inviscid hydraulic theories for rotating channel flow, the potential vorticity of the overflowing fluid (the value at section A of Fig. 3) is often prescribed. Here the potential vorticity is required to be constant at section A to $O(\mathrm{Ro}^2)$ by the geometrical and dynamical constraints of the model. Its value may be expressed in terms of the transport T by inverting (2.5) and substituting the result into (6.2), leading to

$$q_A = \frac{H_E}{H_o}\left[1 - \mathrm{Ro}\frac{H_E}{H_o}\left(\frac{3}{2}(T/W_S)^{2/3} + W_s^2/8\right) + O(\mathrm{Ro}^2)\right]. \tag{8.1}$$

Within the limits of validity of the Rossby number expansion, the potential vorticity decreases for increasing transport. Simply put, large transports lead to large interface displacements above the sill and, since the q_A is dominated by the stretching term [η_g in (6.2)], the result is lower potential vorticity. This trend is consistent with the recent findings of Killworth (1994), which indicate maximal transport for zero potential vorticity. It is possible that this agreement is fortuitous.

9. Open geostrophic contours

If the basin sidewalls are vertical, or are steep enough to be approximated as such, it is possible for them to

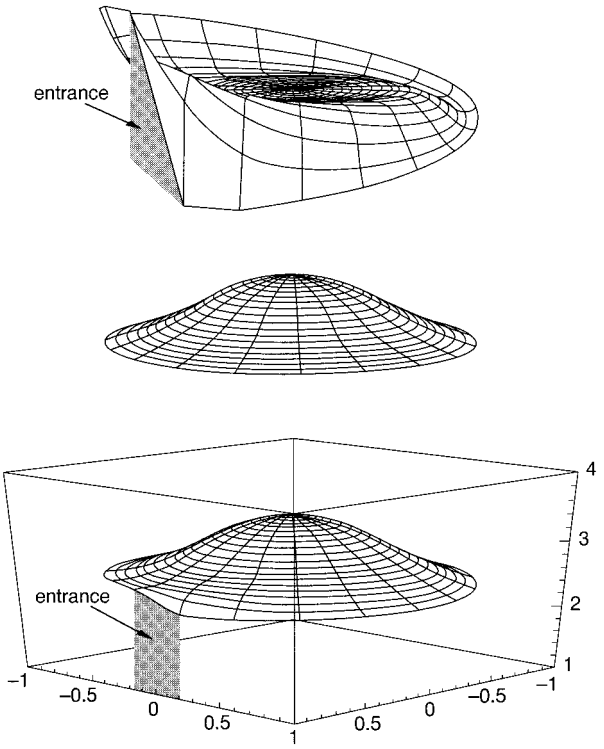

FIG. 5. The top surface represents the interface elevation η_B associated with the (geostrophic) boundary layer fields for the case of interior forcing with the same parameters as in Fig. 4a. The position of the viewer relative to the strait entrance is indicated in Fig. 1. The middle surface is the interior displacement η_g drawn to a larger scale. The lower surface is the sum of η_g and η_B.

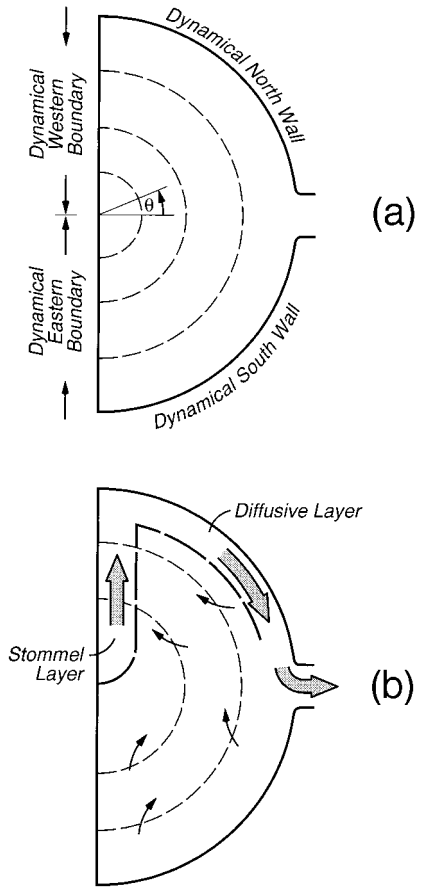

FIG. 6. (a) Sketch of semicircular basin with semicircular bottom contours (dashed) and with vertical wall at left end. (b) The qualitative circulation for a uniformly distributed interior mass source. A Sverdrup interior leads into a Stommel layer on the dynamical western boundary, which in turn leads into a diffusive boundary layer on the north wall.

be intersected by geostrophic contours. As a prototype of this situation consider a semicircular basin with semicircular isobaths, as shown in Fig. 6a. Geostrophic contours intersect the straight section of sidewall lying opposite to the strait. Following a topographic beta-plane analogy the northern (southern) half of this straight section will be called the dynamical western (eastern) boundary since it lies to the left (right) of the direction of decreasing H/H_o. The circulation for this case can be anticipated without having to solve for the details of the flow field.

To lowest order the interface displacement η_o is constant and given by the right-hand side of (3.5). Since the lowest order velocity is zero along boundary-intersecting (open) contours, fluid fed into the interior must make its way to the boundaries via the $O(\varepsilon)$ fields. The radial and azimuthal components of the $O(\varepsilon)$ velocity are now geostrophic since the vanishing of the $O(0)$ velocity removes any friction terms. From (4.1a) the radial velocity reduces to

$$u^{(1)}\frac{\partial}{\partial r}\left(\frac{H}{H_o}\right) = w_p, \tag{9.1}$$

which is essentially the Sverdrup relation for the radial velocity. Fluid introduced from above sets up a cross-isobath flow toward the deeper part of the basin, in this case toward the origin ($r = 0$). Continuity requires that an azimuthal velocity also be set up in order to divert the flow toward the straight boundary. The corresponding boundary layer will essentially be a Stommel layer (of thickness δ_s) and must occur on the dynamical western boundary, as shown in Fig. 6b. After leaving the Stommel layer, the fluid flows toward the strait entrance along the north wall in a diffusive layer with thickness $\tilde{a}^{1/2}\delta_s^{1/2}$ and with dynamics of the type considered in section 6. The south wall also must have a diffusive layer to bring a possibly finite radial transport to zero, as described earlier; however, this layer will carry a relatively small mass flux.

The details of the interior circulation may be determined by calculating the $O(\varepsilon)$ interface displacement from (3.2) of Part I and the geostrophic relations for the $O(\varepsilon)$ velocity. The result is

$$\eta^{(1)}(r, \theta) = \eta_o^{(1)} - \int_{3\pi/2}^{\theta} w_p r \, d\theta', \tag{9.2}$$

where $\eta_o^{(1)}$ is the constant interface displacement along the dynamical eastern boundary ($\theta = 3\pi/2$). The azimuthal velocity is then $v^{(1)} = \partial\eta^{(1)}/\partial r$. The structure of the Stommel layer is well known, and the corresponding solution will be similar to that discussed in section 5e of Pedlosky (1987). The solution for the diffusive layer obeys (5.8) (with $\gamma = 0$) but requires analysis of the upper-left corner region (Fig. 6b) for specification of boundary conditions.

Combinations of open and closed geostrophic contours lead to rich and interesting circulations, many of which can be pieced together using the ideas discussed above. Similar problems have been treated (e.g., Kawase and Straub 1995, manuscript submitted to *J. Phys. Oceanogr.*; Straub et al. 1993) in connection with the abyssal circulation, often with remote sources and interfacial upwelling.

10. A note on horizontal friction

The modeling discussion is concluded with a note on the influence of horizontal friction, which may be a more realistic source of dissipation when the reduced-gravity layer is bounded below by an inactive layer (rather than a solid bottom). In this case $H/H_o = 1$ and $\mathbf{F} = R_e^{-1}$ (F_r, F_θ), where $R_e = A_H/\mathrm{Ro}\, f_o L_d^2$, A_H is the horizontal eddy viscosity, and

$$(F_r, F_\theta) = \nabla^2(u_g, v_g) - \frac{(u_g, v_g)}{r^2} - \frac{2}{r^2}\frac{\partial(v_g, -u_g)}{\partial\theta}.$$

Substituting into (2.3) and using the axisymmetric source (3.2) leads to the equation

$$\frac{\partial}{\partial r}\left(r\frac{\partial v_g}{\partial r}\right) - \frac{v_g}{r} = \frac{T}{4\pi r_o^2}\begin{cases} r^2 T/r_o^2, & r < r_o \\ T, & r > r_o. \end{cases}$$

The solution satisfying the no-slip condition at $r = a$ and which is continuous at $r = r_o$ is

$$v_g = \frac{T}{4\pi r_o^2}\begin{cases} r^3/4 - r_o^2\left(\ln\dfrac{a}{r_o} + \dfrac{r_o^2}{4a^2}\right)r, \\ \qquad r < r_o \\ r_o^4 r^{-1}/4 + r_o^2 r\ln\dfrac{r}{r_o} - r_o^2\left(\ln\dfrac{a}{r_o} + \dfrac{r_o^2}{4a^2}\right)r, \\ \qquad r > r_o, \end{cases} \tag{10.1}$$

giving anticyclonic interior circulation as before.

The boundary layer structure for this case depends upon the bottom topography near the point of intersection with the lower interface. The different possibilities are too lengthy and involved to explore here.

11. Relation to observed phenomena

The basins forming the Norwegian, Iceland, and Greenland Seas confine the deep and, to some extent, the intermediate circulations of the region. What little has been written about the horizontal circulation of deep and intermediate waters is based largely on property distributions and dynamic height calculations. A review of work prior to 1990 is given by Hopkins (1991). Despite the lack of direct velocity measurements, it is interesting to compare inferred circulations to those predicted by the present model. In doing so, it should be noted that the typical slope S of the ridges separating the various basins ranges from 5×10^{-2} to 5×10^{-3} so that fS/D ranges from 0.5×10^{-10} to 5×10^{-11} cm^{-1} s^{-1} when a depth scale $D = 1$ km is used. Since this range is well above the typical value $\beta \approx 10^{-13}$ cm^{-1} s^{-1} for the basins, the f-plane approximation seems reasonable.

Starting with the Greenland Sea, I focus on the Greenland Sea Deep Water (GSDW), which lies below about 2000 m and is topographically confined except for a point in the southeastern part of the basin, where leakage through the Jan Mayen Fracture Zone and into the Norwegian Sea is thought to occur (Aagaard et al. 1985). Debate exists over which mechanism, deep convection or double diffusion and cabbeling, is responsible for GSDW formation, but the most recent and highest precision property measurements suggest that the former is dominant (Clarke et al. 1990). Forcing due to an interior mass source would therefore seem the most appropriate for the present model. In this case Eq. (3.1) predicts anticyclonic deep flow in the basin interior, a finding neither confirmed nor disputed by observation. (Deep inflow from the Arctic is thought to circulate *cyclonically* about the west and south edges of the basin but this flow does not lie below the region of suspected convection.)

Turning to the deep waters of the Norwegian Sea, the primary source appears to be the aforementioned inflow through the Jan Mayen Fracture Zone (Aagaard et al. 1985), whereas the primary sink is the Faroe–Shetland Channel. Since only upper deep water is found in the latter, the most realistic model configuration may consist of a reduced-gravity layer with ''floating'' upper and lower interfaces, the lower boundary contacting the bottom only at the sloping basin edge. Also since deep convection does not occur in the Norwegian Sea, the most realistic model forcing consists of side wall sources and sinks. Figure 7 shows the horizontal circulation in a circular basin created by a isolated source at the northern tip (the Jan Mayen Fracture Zone inflow) and an outflow at the southern tip (the Faroe–Shetland Channel). The depth and width of the entrance and exit gaps are assumed to be the same. All parameters are the same as for the case, Fig. 4b, except that the source is concentrated in uniform inflow of width W = 0.5, leading to the Fourier coefficients $A_0 = B_n = 0$ and

$$A_n = \frac{4TH_o}{\pi WH_e}\sum_{n=1,3,5,\ldots}^{\infty}\frac{1}{n}\sin\frac{nW}{2a}$$

in (7.2). As shown, the throughflow is concentrated in

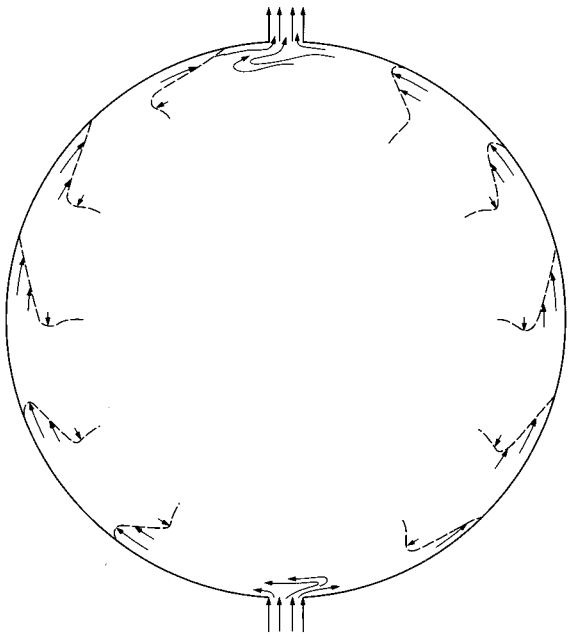

FIG. 7. Flow fed by isolated source and sink. The parameters are identical to the Fig. 4b flow, and the width of the source is $W = 0.5$.

boundary layers on either side of the basin. Although the two layers are not symmetric, the mass flux is equally divided between them. Note that the flow approaching the sink from the west overshoots, as was true in the second case (Fig. 4).

The lack of deep interior circulation within the Norwegian Sea is supported by the flat potential density contours in the sections published by Clarke et al. (1990), provided a deep reference level exists. The lack of interior mean currents is also supported by a current meter record obtained by Sellmann et al. (1992). The Norwegian Sea is separated into two basins, the Norwegian Basin to the southwest and the Lofoten Basin to the northeast. Mauritzen (1993) cites hydrographic sections in the Lofoten Basin indicating a boundary current, possibly anticyclonic in direction, which would correspond to the eastern boundary current in the model (Fig. 7). This structure is not present in all sections. There is also evidence for cyclonic flow in the Norwegian Basin (Saelen 1986), which could be the predicted western boundary current.

Applying the model to the Iceland Sea is more problematic due, in part, to the fact that convection leads to intermediate waters that lie above 500 m or so (Swift and Aagaard 1981) and are not topographically confined to the extent of the deep water. It is therefore questionable whether a basin geometry is the most appropriate setting. Also, there are differences in opinion as to the fate of the intermediate water, Swift and Aagaard (1981) believing it to exit through the Denmark Strait and Mauritzen (1993; 1996a,b) believing it to flow east into the Norwegian Sea. The dynamic topography relative to 800 dbar indicates cyclonic flow at the surface (Swift and Aagaard 1981), and the present model as well as that of Gill et al. (1979), predicts an intermediate anticyclone, at least in the absence of wind forcing.

It is notable that deep anticyclones in regions of thermal convection are predicted by a number of models (e.g., Gill et al. 1979) but generally not (yet?) observed.

12. Eastern versus western boundary currents

What determines the sense (anticyclonic or cyclonic) and the distribution (eastern vs western) of the boundary flow and how sensitive are these features to variable Coriolis acceleration? Some insight into this question can be gained by forming a circulation integral for the entire basin. Consider the potential vorticity equation (5.2) generalized to include y-varying f, obtained by replacing $(1 + \mathrm{Ro}\zeta)$ by $(f(y)/f_o + \mathrm{Ro})$. Multiplying the result by the $(H/H_o + \mathrm{Ro}\eta)$, integrating over the area A of the basin, and making use of mass conservation leads to

$$\oint_{\partial A} \left(\frac{f(y)}{f_o} + \mathrm{Ro}\zeta \right) \mathbf{u}\cdot\mathbf{n}\, ds = \mathrm{Ro} \oint_{\partial A} \frac{\mathbf{F}H_o}{H}\cdot\mathbf{l}\, ds, \quad (12.1)$$

where ∂A represents the basin edge. Equation (12.1) expresses a balance between the net horizontal input of planetary and relative vorticity by the normal velocity $-\mathbf{u}\cdot\mathbf{n}$ and dissipation of vorticity about the basin edge. Under the linear drag law $\mathbf{F} = -R_f\mathbf{u}$ and thus the dissipation is proportional to the tangential velocity at the basin edge. Also, the inflow/outflow velocity is $O(\mathrm{Ro})$ by assumption, and thus the lowest order circulation balance is

$$\oint_{\partial A} \frac{f(y)}{f_o}\mathbf{u}\cdot\mathbf{n}\, ds = -R_f \oint_{\partial A} \frac{H_o}{H}\mathbf{u}\cdot\mathbf{l}\, ds. \quad (12.2)$$

Suppose first that the flow is fed from above and that the basin is drained by a single strait. Also suppose that $f(y)$ and H are approximately constant across the strait entrance with average values f_1 and H_1, say. Then (12.2) reduces to

$$\frac{f_1 H_o T}{f_o H_1} = -R_f \oint_{\partial A} \frac{H_o}{H}\mathbf{u}\cdot\mathbf{l}\, ds, \quad (12.3)$$

where, again, T is the (positive) volume transport exiting the basin. Thus the tangential velocity $\mathbf{u}\cdot\mathbf{l}$ must be generally negative about the basin edge, suggesting overall anticyclonic flow, as in the example (Fig. 5).

If instead the flow is fed by a single lateral inflow and drained by a single outflow (Fig. 7), (12.2) becomes

$$\left(\frac{f_1 H_o}{f_o H_1} - \frac{f_2 H_o}{f_o H_2} \right) T = -R_f \oint_{\partial A} \frac{H_o}{H}\mathbf{u}\cdot\mathbf{l}\, ds, \quad (12.4')$$

where the subscript 2 denotes the source strait and 1 the sink strait. If $f_1 = f_2$ and $H_1 = H_2$, as in the Norwegian Sea example, the left-hand side of (12.4) van-

ishes and thus the right-hand circulation integral must also vanish. The boundary flow must therefore be cyclonic ($\mathbf{u}\cdot\mathbf{l} > 0$) over a portion of the basin edge and anticyclonic ($\mathbf{u}\cdot\mathbf{l} < 0$) elsewhere. With the two straits on opposite sides of the basin the simplest scenario is for the entering flow to split and form two boundary currents, one cyclonic and one anticyclonic, as in Fig. 7. The feature of balancing cyclonic and anticyclonic boundary flow can be generalized to any lateral source/sink distribution provided f and H are constant around the basin edge. The central idea is that no net planetary vorticity is introduced and therefore the net dissipation must vanish.

If the values of f_1 and f_2 differ, as would occur on a β plane with the straits at different latitudes, then the left-hand side of (12.4) is no longer zero. In physical terms, the influx of planetary vorticity at the source strait is different from that at the sink strait. A similar effect is created if H_1 and H_2 differ, as in a topographic β plane, for then $\int \mathbf{u}\cdot\mathbf{n}\, ds$ differs between the two straits, implying differing fluxes of f. As an example, consider the two strait solution, Fig. 7, as modified by a slight difference in f between the northern and southern strait. If f_2, the value of f at the northern strait, is slightly larger than f_1 and H is constant around the basin edge, then $\oint_{\partial A} \mathbf{u}\cdot\mathbf{l}\, ds$ is positive but small according to (12.4). Thus we may expect a slight intensification in the boundary current on the western side of the basin relative to the eastern side. Increasing the difference between f_2 and f_1 should increase the westward intensification in agreement with conventional wisdom regarding western boundary layers.

In the Norwegian Sea example (Fig. 7) H_1 was arbitrarily chosen to be equal to H_2, largely because discriminatory observational evidence does not exist. However, mismatches between the two would lead to differences between the eastern and western boundary currents.

13. Limitations and future improvements

The assumption of reduced-gravity dynamics is somewhat limiting. For example, the Norwegian Sea Upper Deep Water is overlain by an intermediate water mass, which also participates in the Faroe–Shetland overflow and may exert influence on the deeper flow. Future improvements to the model should include adding an active upper layer. Also Johnson and Ohlsen (1994), Johnson and Sanford (1992), and Pratt (1986) have pointed out the limitations of using frictionless hydraulic models in the Faroe Bank Channel. In fact, Whitehead (1989) has compared the volume outflow predicted by the WLK model to observed values and found that the theory overestimates the observations by 160%–400%. Addition of friction would presumably lower the predicted values.

Another limitation of the present model is the treatment near the ''basin edge,'' where the lower-layer depth vanishes. A certain amount of complication has been avoided by representation of bottom drag as a body force and the artificial use, in some cases, of a vertical wall. As pointed out by MacCready and Rhines (1991) [and reviewed by Garrett et al. (1993)] the cross-slope advection of density by the bottom Ekman layer can lead to stress-free conditions at the edge of the flow. This situation is avoided in the reduced-gravity formulation since the Ekman layer (or body force representation thereof) is homogeneous. However, the presence of continuous stratification might be expected to produce a boundary stress distribution qualitatively different than the one imposed here.

Acknowledgments. This work was supported by the National Science Foundation under Grant OCE 9115359 and the Office of Naval Research under Grant N00014-95-1-0456. The author would like to thank Cecilie Mauritzen for helpful discussions concerning section 11 and Joe Pedlosky for a suggestion that lead to some of the formulations in section 12.

REFERENCES

Aagaard, K., J. H. Swift, and E. C. Carmack, 1985: Thermohaline circulation in the Arctic mediterranean seas. *J. Geophys. Res.*, **90**(C3), 4833–4845.

Clarke, A. R., J. H. Swift, J. L. Reid, and K. P. Koltermann, 1990: The formation of Greenland Sea Deep Water: Double diffusion or deep convection. *Deep-Sea Res.*, **37,** 1385–1424.

Csanady, G. T., 1978: The arrested topographic wave. *J. Phys. Oceangr.*, **8,** 47–62.

Garrett, C., P. MacCready, and P. Rhines, 1993: Boundary mixing and arrested Ekman layers: Rotating stratified flow near a sloping boundary. *Annu. Rev. Fluid Mech.*, **25,** 291–323.

Gill, A. E., J. M. Smith, R. P. Cleaver, R. Hide, and P. R. Jonas, 1979: The vortex created by mass transfer between layers of a rotating fluid. *Geophys Astrophys. Fluid Dyn.*, **12,** 195–220.

Hopkins, T. S., 1991: The GIN Sea—A synthesis of its physical oceanography and literature review. 1972–1985. *Earth-Sci. Rev.*, **30,** 175–318.

Johnson, J. C., and T. B. Sanford, 1992: Secondary circulation in the Faroe Bank Channel outflow. *J. Phys. Oceanogr.*, **22,** 928–932.

——, and D. R. Ohlsen, 1994: Frictionally modified rotating hydraulic channel exchange and ocean outflows. *J. Phys. Oceanogr.*, **24,** 66–78.

Killworth, P. D., 1994: On reduced-gravity flow through sills. *Geophys. Astrophys. Fluid Dyn.*, **75,** 91–106.

MacCready, P., and P. Rhines, 1991: Buoyant inhibition of Ekman transport on a slope and its effect on stratified spin-up. *J. Fluid Mech.*, **223,** 631–661.

Mauritzen, C., 1993: A Study of the large scale circulation and water mass formation in the Nordic seas and Arctic Ocean. Ph. D. thesis, WHOI/MIT Joint Program, 211 pp.

——, 1996a: Production of dense overflow waters Feeding the North Atlantic across the Greenland–Scotland Ridge. Part I. Production of dense overflow waters feeding the North Atlantic across the Greenland–Scotland Ridge. *Deep-Sea Res.*, **43B,** 769–806.

——, 1996b: Evidence for a revised circulation scheme. Part II: An inverse model. *Deep-Sea Res.*, **43B,** 807–835.

Pedlosky, J., 1968: An overlooked aspect of wind-driven oceanic circulation. *J. Fluid Mech.*, **43,** 809–821.

——, 1974: Longshore currents, upwelling and bottom topography. *J. Phys. Oceanogr.*, **4,** 214–216.

——, 1987: *Geophysical Fluid Dynamics.* Springer-Verlag, 710 pp.

Pratt, L. J., 1986: Hydraulic control of sill flow with bottom friction. *J. Phys. Oceanogr.,* **16,** 1970–1980.

——, 1987: Rotating shocks in a separated laboratory channel flow. *J. Phys. Oceanorgr.,* **17,** 483–491.

——, and S. G. Llewellyen Smith, 1997: Hydraulically drained flows in rotating basins. Part I: Method. *J. Phys. Oceanogr.,* **27,** 2509–2521.

Saelen, O. H., 1986: On the exchange of bottom water between the Greenland and Norwegian Seas. *Nordic Perspectives on Oceanography, Geophysica,* **3,** 133–144.

Sellmann, L., E. Fahrbach, G. Rohardt, V. H. Strass, and B. v. Bodungen, 1992: Moored instruments oceanographic data from the Greenland Sea 1987–1989. *AWI Ber. Fachber. Physik,* Alfred-Wegener-Institut für Polar- und Meeresforschung, Vol. 27, 120 pp.

Shen, Y.-C., 1981: The rotating hydraulics of open-channel flow between two basins. *J. Fluid Mech.,* **112,** 161–188.

Straub, D. N., P. D. Killworth, and M. Kawase, 1993: A simple model of mass-driven abyssal circulation over a general bottom topography. *J. Phys. Oceanogr.,* **23,** 1454–1459.

Swift, J. H., and K. Aagaard, 1981: Seasonal transitions and water mass transformations in the Iceland and Greenland Seas. *Deep-Sea Res.,* **28,** 1107–1129.

Whitehead, J. A., 1989: Internal hydraulic control in rotating fluids—Applications to the oceans. *Geophys. Astrophys. Fluid Dyn.,* **48,** 169–192.

——, A. Leetma, and R. A. Knox, 1974: Rotating hydraulics of strait and sill flows. *Geophys. Fluid Dyn.,* **6,** 101–125.